

## The two-dimensional double layered antiferromagnet $\text{Rb}_3\text{Mn}_2\text{Cl}_7$ —a neutron diffraction study

E. Gurewitz and J. Makovsky

*Nuclear Research Centre-Negev, Post Office Box 9001, Beer-Sheva, Israel*

H. Shaked

*Nuclear Research Centre-Negev, Post Office Box 9001, Beer-Sheva, Israel*

*and Ben Gurion University-Negev, Post Office Box 2053, Beer-Sheva, Israel*

(Received 26 November 1975)

The structure of  $\text{Rb}_3\text{Mn}_2\text{Cl}_7$  is similar to that of  $\text{Rb}_2\text{MnCl}_4$ . Whereas in  $\text{Rb}_2\text{MnCl}_4$  there are single  $\text{MnCl}_2$  layers which are shifted one from the other by the  $(1/2, 1/2, 1/2)$  translation, in  $\text{Rb}_3\text{Mn}_2\text{Cl}_7$ , instead of single layers there are pairs of layers. In the temperature range  $64.5 < T < 100^\circ\text{K}$  the crystal behaves like a two-dimensional antiferromagnet. Its magnetic moments are oriented along the  $c$  axis. Every moment is antiparallel to its five  $\text{Mn}^{2+}$  nearest neighbors. In this temperature range there are no correlations between the various pairs of layers. Therefore, instead of points in the reciprocal space one expects to obtain rods of reflections along  $c^*$ , as in the case of the single-layer type compounds. In the double-layer case, however, one expects the intensity of the rods to be modulated with a wave vector  $2\pi/t$  where  $t$  is the intrapair distance between layers. Several scans made along and across the  $(0, 1, l)$  rods confirmed these expectations. Below  $T_N \sim 64.5^\circ\text{K}$  the compound orders in three dimensions and as in  $\text{Rb}_2\text{MnCl}_4$  we find here (the same kind of) magnetic polytypism.

### I. INTRODUCTION

The compound  $\text{Rb}_3\text{Mn}_2\text{Cl}_7$  belongs to a family of compounds with the formula  $A_{n+1}B_nX_{3n+1}$ , where  $A$ ,  $B$  and  $X$ , are alkali metal, transition metal, and a halogen or oxygen, respectively. The crystallographic structures in this family belong to the tetragonal space group  $D_{4h}^{17}-I4/mmm$  with two molecules per unit cell.<sup>1</sup> In these structures, the  $B^{2+}$  ion is located at the center of an octahedron of  $X^-$  ions. This is shown for  $n=2$  in Fig. 1. The structure consists of two sets of  $2n+1$  layers ( $n+1$  layers of  $AX$  and  $n$  layers of  $BX_2$ ) connected through the body-center translation. The dimensions of the unit cell are determined by the ionic radii of the  $A^+$  and the  $X^-$  ions which are at least twice those of the  $B^{2+}$  ions. Hence, an ideal lattice with lattice translation  $a_c$  and  $c_c$  is defined as one with ideal  $X^-$  octahedra  $a_c/\sqrt{2}$  on edge and an  $AX$  interlayer distance of the same length. Choosing the origin of the unit cell at the lower apex of an octahedron of the lowest layer in a set leads to the ideal positions of the ions as given in Table I. The ideal  $c_c/a_c$  ratio is  $(c_c/a_c)_{\text{ideal}} = 2n + \sqrt{2}$ . A comparison of the ideal to observed  $c/a$  parameters is given in Table II for two systems<sup>2</sup> with  $n=1, 2, 3$ . In these and many other compounds we have found<sup>3</sup> that the observed  $c/a$  and the observed ionic parameter values are in good agreement with the corresponding ideal values.

On the basis of magnetic structures reported<sup>4</sup> for  $(n=1)$ -type compounds we expect the magnetic structures in the  $(A_{n+1}B_nX_{3n+1})$ -type compounds to be as follows: (a) Intralayer nearest-neighbor (nn) inter-

actions are antiferromagnetic. Hence, the basal-plane translations of the magnetic lattice  $\vec{a}_m$  and  $\vec{b}_m$  are given by

$$\vec{a}_m = \vec{a}_c + \vec{b}_c, \quad \vec{b}_m = \vec{a}_c - \vec{b}_c.$$

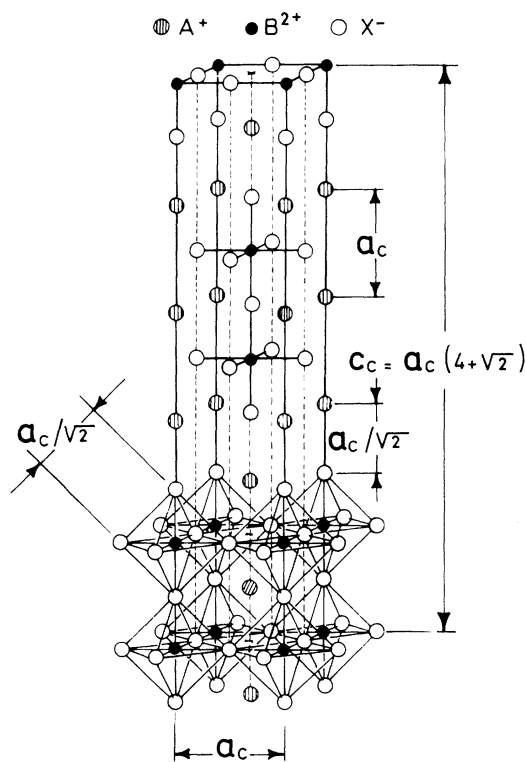


FIG. 1. Crystallographic structure of an ideal  $n=2$  (double layered) compound.

TABLE I. Positions of the ions of one unit formula  $A_{n+1}B_nX_{3n+1}$  compounds in an ideal unit cell.<sup>a</sup>

Ion	Coordinates in the unit cell <sup>b</sup>	Ideal value (in units of $a/c$ ) of the $z$ parameter	Values of $m$
$A^+$	$\frac{1}{2}, \frac{1}{2}, z$	$m$	$0, \dots, n-1, n$
$B^{2+}$	$0, 0, z$	$\frac{1}{2}(2m+1)$	$0, \dots, n-1$
$X^-$	$0, 0, z$	$m$	$0, \dots, n-1, n$
$X^-$	$0, \frac{1}{2}, z \quad \frac{1}{2}, 0, z$	$\frac{1}{2}(2m+1)$	$0, \dots, n-1$

<sup>a</sup> The two unit formulas are connected thru the  $(\frac{1}{2}, \frac{1}{2}, \frac{1}{2})$  translation.

<sup>b</sup> The origin of the unit cell was chosen to be at the lower apex of an octahedron at the lowest layer in a set.

(b) Interactions between nearest sets (connected through  $I$  translation), vanish owing to symmetry. (c) Interactions between next-nearest sets (i.e., sets connected thru  $c_c$  translation) are weak due to the long interset distance. (d) Owing to the similarity of the inter- (within a set) and intralayer geometry (Fig. 1), the interlayer  $m$  interaction within a set is expected to be antiferromagnetic. (e) The spin axis is along the unique axis (see Sec. III).

The above features give rise to a magnetic two-dimensional behavior<sup>4</sup> and magnetic polytypism<sup>5</sup> which were observed in ( $n=1$ )-type structures. Magnetic two-dimensional behavior and polytypism are reported for the first time in this paper for ( $n=2$ )-type (double layered) structures.

## II. PREPARATION AND CRYSTALLOGRAPHY

Samples of  $Rb_3Mn_2Cl_7$  were prepared in two different methods: (a) The molten salt method<sup>6</sup> (MS). (b) The aqueous or alcoholic solution method<sup>5</sup> (AS).

Neutron diffraction patterns of the MS and AS samples taken at room temperature (RT) are shown in Fig. 2. The patterns are indexed according to the chemical lattice constants<sup>7</sup>  $a_c = 5.05 \text{ \AA}$  and  $c_c = 26.14 \text{ \AA}$ . These patterns, as well as x-ray

TABLE II. Ideal to observed  $c/a$  ratio, for the two systems (Ref. 2) CaO-MnO; SrO-MnO.

$n$	Compound	$c/a$	
		Observed	Ideal
1	$Ca_2MnO_4$	3.29	3.14
	$Sr_2MnO_4$	3.25	
2	$Ca_3Mn_2O_7$	5.25	5.14
	$Sr_3Mn_2O_7$	5.23	
3	$Ca_4Mn_3O_{10}$	7.21	7.14
	$Sr_4Mn_3O_{10}$	7.21	

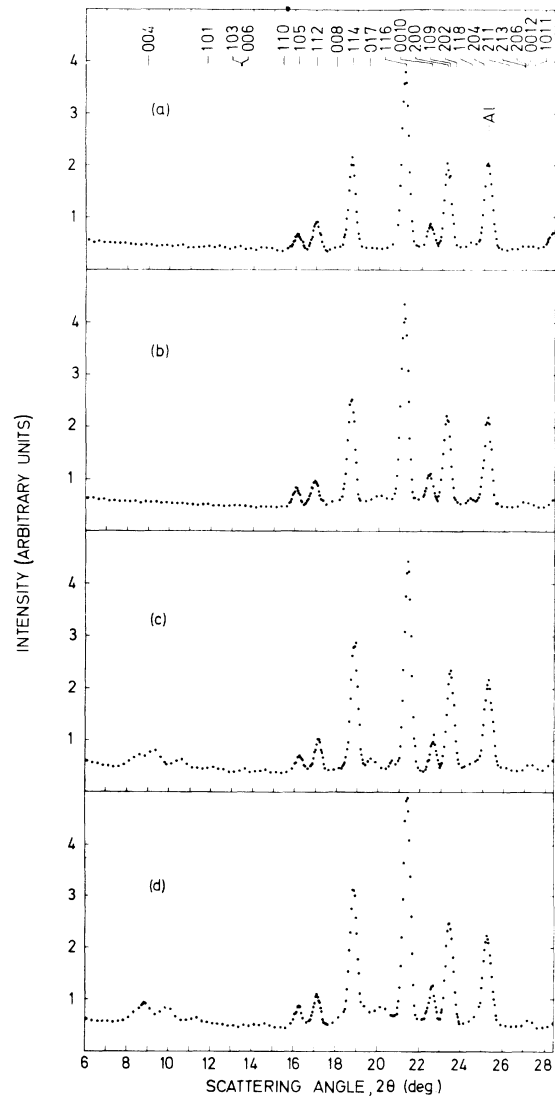


FIG. 2. Neutron ( $\lambda \sim 1.02 \text{ \AA}$ ) diffraction patterns of (a) MS and (b) AS samples taken at RT and of (c) MS and (d) AS samples taken at LHeT. Indexing is according to the chemical lattice constants  $a_c = 5.05$  and  $c_c = 26.14 \text{ \AA}$ .

TABLE III. Results of the least squares analysis.<sup>a</sup> Parameters for the MS and AS samples of  $\text{Rb}_3\text{Mn}_2\text{Cl}_7$  at room temperature and liquid-helium temperature which were used to obtain  $I_{\text{calc}}$  in Tables IV–VII.

Ion	Ideal value	Room temperature		Liquid-helium temperature	
		MS	AS	MS	AS
$\text{Rb}^+$	0.184	$0.180 \pm 0.002$	$0.179 \pm 0.002$	$0.176 \pm 0.002$	$0.176 \pm 0.003$
$\text{Mn}^{2+}$	0.359	$0.398 \pm 0.005$	$0.400 \pm 0.005$	$0.399 \pm 0.003$	$0.395 \pm 0.007$
$\text{Cl}_{\text{II}}^-$	0.306	$0.303 \pm 0.002$	$0.305 \pm 0.002$	$0.297 \pm 0.001$	$0.301 \pm 0.002$
$\text{Cl}_{\text{III}}^-$	0.092	$0.094 \pm 0.001$	$0.094 \pm 0.001$	$0.095 \pm 0.001$	$0.094 \pm 0.002$
Number of Bohr magnetons				$4.2 \pm 0.2$	$4.3 \pm 0.2$

<sup>a</sup> Using the scattering amplitudes published by the Neutron Diffraction Commission [Acta Crystallogr. A **28**, 357 (1972)], and the atomic form factors published by R. W. Watson and A. J. Freeman [Acta Crystallogr. **14**, 27 (1961)].

data, did not reveal any significant difference between the two samples.

The parameters which yielded the best fit of the calculated to integrated intensities of 14 lines observed at RT are listed in Table III. The observed integrated intensities of these lines are compared with the intensities calculated for these parameters in Table IV. The parameters obtained for the two different preparations are equal within error limits. Similar parameters were obtained for the samples at liquid-helium temperature (LHeT) and are given in Tables V–VII.

### III. ANALYSIS AND DISCUSSION OF THE MAGNETIC STRUCTURE

Neutron diffraction patterns were obtained with the MS and AS samples at LHeT and are shown in Figs. 2 and 3. A comparison of the RT and the LHeT patterns shows that the LHeT patterns contain several lines which were absent in the RT patterns. The indices of the new lines are  $\{\frac{1}{2} \frac{1}{2} l\}$  with  $l$  an integer and  $\{\frac{1}{2} \frac{1}{2} (\frac{1}{2} l)\}$  with  $l$  an odd integer for the MS and the AS samples, respectively.

From this we conclude that the translations of

TABLE IV. Comparison of calculated and observed integrated intensities of nuclear reflections<sup>a</sup> of neutrons from MS and AS  $\text{Rb}_3\text{Mn}_2\text{Cl}_7$  powder samples at room temperature.

$\{hkl\}$	MS		AS	
	$I_{\text{obs}}$	$I_{\text{calc}}$	$I_{\text{obs}}$	$I_{\text{calc}}$
004	$0 \pm 2$	0.4	$0 \pm 2$	0.8
101	$0 \pm 2$	1.9	$0 \pm 2$	1.8
103, 006	$5 \pm 4$	2.8	$3 \pm 2$	3.2
105, 110	$31 \pm 4$	27.6	$40 \pm 4$	27.6
112	$51 \pm 4$	44.3	$45 \pm 4$	43.4
008	$5 \pm 2$	4.4	$6 \pm 3$	4.3
114	$170 \pm 4$	171.6	$169 \pm 6$	163.4
116	$297 \pm 6$	302.5	$309 \pm 8$	310.5
0010	$46 \pm 3$	50.5	$39 \pm 4$	48.5
200, 109, 202	$146 \pm 5$	137.8	$138 \pm 5$	136.2
118	$15 \pm 3$	11.3	$12 \pm 3$	109.5
211	$0 \pm 2$	0.8	$0 \pm 2$	0.8
213, 206, 0012, 1011	$16 \pm 5$	14.6	$15 \pm 5$	15.4
217	$0 \pm 2$	3.5	$0 \pm 2$	2.8
Weighted $R$ factor (Ref. 8)		0.05		0.08

<sup>a</sup> All the allowed reflections in the range  $9.5 \text{ \AA} \geq d \geq 1.85 \text{ \AA}$  were included except for  $\{204\}$  and  $\{208\}$  which are obscured by the  $\{111\}$  and  $\{200\}$  reflections, respectively, and  $\{215\}$  which is suspected of including some contaminations of  $\text{RbCl-MnCl}_2$  phase.

TABLE V. Comparison of calculated and observed integrated intensities of nuclear reflections<sup>a</sup> of neutron MS and AS Rb<sub>3</sub>Mn<sub>2</sub>Cl<sub>7</sub> powder samples at liquid-helium temperature.

$\{hkl\}$	MS		AS	
	$I_{\text{obs}}$	$I_{\text{calc}}$	$I_{\text{obs}}$	$I_{\text{calc}}$
101	0 ± 2	3.7	0 ± 2	3.0
103, 006	4 ± 4	3.4	3 ± 2	3.6
105, 110	36 ± 5	36.7	31 ± 5	36.2
112	51 ± 4	52.5	47 ± 4	49.8
008	5 ± 4	4.9	4 ± 3	2.8
114	220 ± 6	214.9	213 ± 8	201.1
116	330 ± 7	325.1	351 ± 10	337.5
0010	48 ± 3	54.2	43 ± 4	53.9
200, 109, 202	169 ± 4	171.7	165 ± 5	164.9
118	11 ± 4	8.2	10 ± 3	10.6
211	0 ± 2	1.6	0 ± 2	1.2
213, 206, 0012, 1011	17 ± 4	19.3	16 ± 4	19.2
Weighted $R$ factor (Ref. 8)		0.04		0.08

<sup>a</sup> All the allowed reflections in the range  $9.5 \text{ \AA} \geq d \geq 2.1 \text{ \AA}$  were included except those excluded in Table I and  $\{004\}$  which is obscured by magnetic reflections.

the chemical lattice  $a_c$  and  $b_c$  change to antitranslations in the magnetically ordered state. The interaction between  $mm$  (Figs. 1 and 4) is therefore antiferromagnetic. The magnetic lattice translations are given by

$$\vec{a}_m = \vec{a}_c + \vec{b}_c, \quad \vec{b}_m = \vec{a}_c - \vec{b}_c$$

for the two samples, where

$$\vec{c}_m = \vec{c}_c, \quad \vec{c}_m = 2\vec{c}_c$$

for the MS and AS samples, respectively.

Hence, the volume of the magnetic unit cell is two and four times the volume of the chemical unit cell in the MS and the AS samples, respectively.

An analysis of the observed magnetic intensities of the two samples (Tables VI and VII) shows that: (a) The two layers of a set are coupled antiferromagnetically. (b) The antiferromagnetic axis is parallel to  $\vec{c}_c$ . (c) The magnetic moment per Mn<sup>2+</sup>

ion calculated from 4.2 °K patterns (Table III) is  $4.2 \pm 0.2$  and  $4.3 \pm 0.2$  Bohr magnetons for the MS and AS samples, respectively.

The two corresponding magnetic structures are shown in Fig. 4. The magnetic space groups<sup>9</sup> are  $F_C m' m' m'$  ( $F_B m' m' m'$  in our setting) and  $P_I 4_2/m' m' m'$  for the MS and AS samples respectively (these correspond to Shubnikov groups<sup>10</sup>  $\text{III}_{68}^{520}$  or  $C_A cca$  and  $\text{III}_{141}^{570}$  or  $I_C 4_1/acd$ , respectively). The respective decrease in symmetry from the paramagnetic space group  $1'14/mmm$  is the same for the two structures and is equal to four. The two interlaced magnetic lattices in the MS structure are connected thru  $(\frac{1}{2}, 0, \frac{1}{2}) \times 1'$  and  $(0, \frac{1}{2}, \frac{1}{2})$ , whereas in the AS structure there is no symmetry element connecting the two interlaced magnetic lattices.

With  $B = \text{Mn}^{2+}$ , the dominant term in the magnetic anisotropy energy is<sup>11</sup> the dipolar term  $E_{\parallel} - E_{\perp}$  (the indices correspond to spin, parallel and perpen-

TABLE VI. Comparison of calculated and observed integrated intensities of magnetic reflections of neutrons from an MS powder sample at liquid-helium temperature.

$\{hkl\}$ <sup>a</sup>	$I_{\text{obs}}$	$I_{\text{calc}}$
011	26 ± 4	25.0
102	45 ± 4	43.4
013	20 ± 4	24.6
104	3 ± 2	4.9
015	0 ± 2	0
Weighted $R$ factor (Ref. 8)		0.110

<sup>a</sup> The indices are with respect to the magnetic unit cell.

TABLE VII. Comparison of calculated and observed integrated intensities of magnetic reflections of neutrons from an AS powder sample at liquid-helium temperature.

$\{hkl\}$ <sup>a</sup>	$I_{\text{obs}}$	$I_{\text{calc}}$
101, 103	59 ± 9	53.4
105	39 ± 5	41.2
107	8 ± 5	14.6
109	0 ± 2	1.0
Weighted $R$ factor (Ref. 8)		0.140

<sup>a</sup> The indices are with respect to the magnetic unit cell.

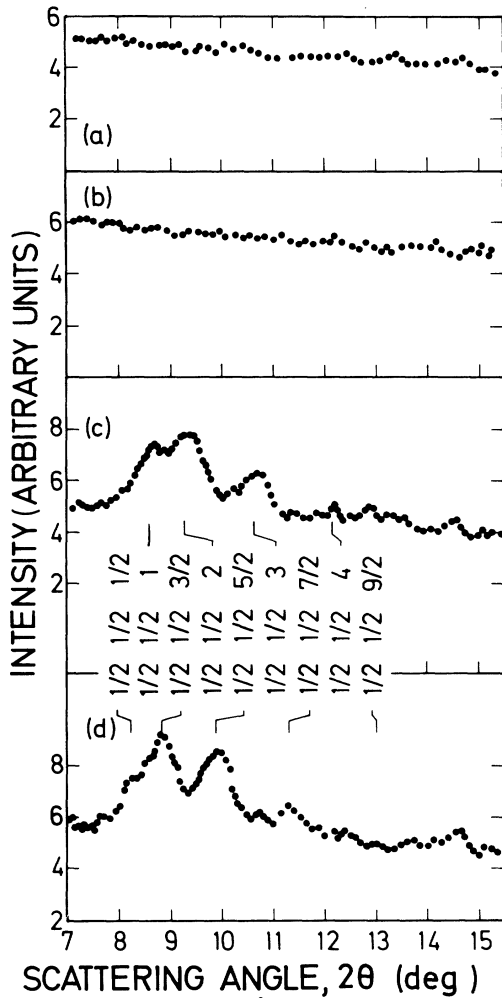


FIG. 3. Neutron ( $\lambda \sim 1.02 \text{ \AA}$ ) diffraction patterns of (a) MS and (b) AS samples taken at RT and of (c) MS and (d) AS samples taken at LHeT. Indexing is according to the chemical lattice constants.

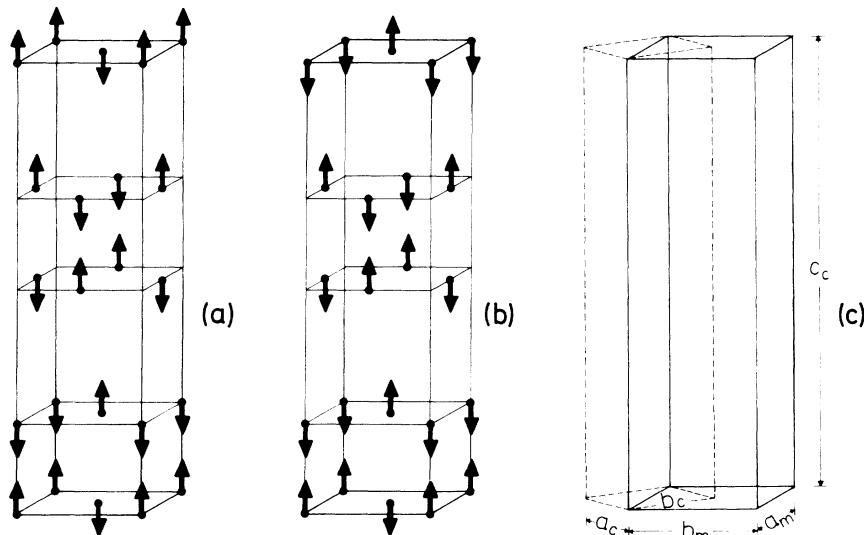


FIG. 4. Magnetic structure of the (a) MS and (b) AS (half a unit cell!) samples. Connection between the chemical and magnetic cells is shown in (c).

dicular to the unique axis). For these structures  $E_{\parallel} = -2E_{\perp}$ ,<sup>12</sup> hence the anisotropy energy is equal to  $\frac{3}{2}E_{\parallel}$ .

Let  $\epsilon_0$  and  $\epsilon_1$  be the contributions to the dipolar energy of an ion, which come from its own layer and its first neighbor layer, respectively. Contributions from other layers are small and can be neglected. The average dipolar energy per ion,  $\langle E_D \rangle$ , in a crystal with sets of  $n$  layers is therefore given by

$$n \langle E_D \rangle = n\epsilon_0 + 2(n-1)\epsilon_1.$$

In the "parallel" case, numerical calculations with an ideal lattice yield  $\epsilon_1 \sim -\frac{1}{2}\epsilon_0$ , hence

$$\langle E_D \rangle_{\parallel} \sim \epsilon_0/n.$$

Numerical calculations in ideal lattices with  $n = 1, 2, 3, 4, 5$  are in excellent agreement with the latter equation and yield  $\epsilon_0 = 33 \times 10^{-18}$  erg for  $a_c = 5 \text{ \AA}$ . It is seen that the anisotropy energy  $\frac{3}{2}\langle E_D \rangle_{\parallel}$ , decreases as  $n$  increases and goes to zero as  $n \rightarrow \infty$  (cubic perovskite) as expected. Hence, the anti-ferromagnetic axis is expected to be along the unique axis as long as  $n$  is not too large so that the anisotropy energy  $\frac{3}{2}\langle E_D \rangle_{\parallel}$  is the dominant term.

The existence of two different magnetic structures depending on the method of preparation is known<sup>5</sup> to occur in several  $n=1$  compounds ( $\text{Rb}_2\text{MnCl}_4$  and  $\text{Rb}_2\text{MnF}_4$ ), and was termed magnetic polytypism. It was argued<sup>5</sup> that magnetic polytypism may occur in the layered ( $A_{n+1}B_nX_{3n+1}$ )-type compounds. Magnetic polytypism in  $\text{Rb}_3\text{Mn}_2\text{Cl}_7$ , which is reported here, is the first case of polytypism found in an ( $n=2$ )-type compound.

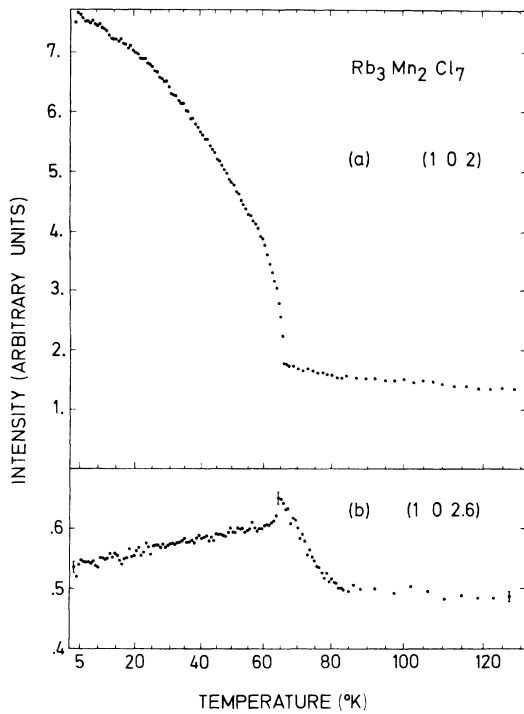


FIG. 5. Temperature dependence of the peak intensity at the (a) Bragg position (102) and (b) off Bragg position at (10 2.6) from a single crystal prepared by the MS method. Indices are according to the MS magnetic lattice.

#### IV. CRITICAL SCATTERING

The peak-intensity temperature curve for the (102) magnetic reflection of a single crystal prepared by the MS method is shown in Fig. (5a). The transition temperature exhibited by this curve is at  $T \sim 64.5^\circ\text{K}$ . Some residual intensity prevails

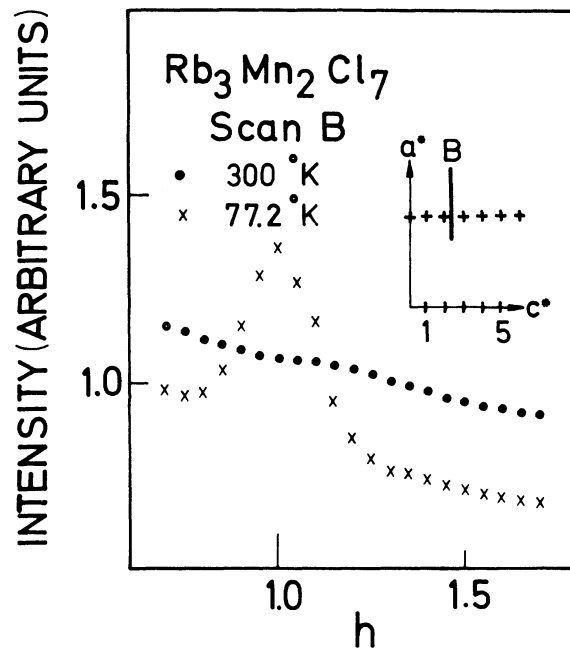


FIG. 7. Scans in reciprocal space across the rod  $(h, 0, l)$  at  $l=2.2$ .

above  $T_N$  up to about  $90^\circ\text{K}$ . This is critical scattering due to time and space fluctuations in the sublattice magnetization of domains which are small far from  $T_N$  and become very large as  $T_N$  is approached. The critical scattering can be better seen in an off Bragg position as is shown in Fig. (5b). As was already mentioned, we expect two-dimensional behavior in these compounds as was found for several ( $n=1$ )-type compounds (i.e., correlations within the layers with no correlation between layers). Such a behavior is manifested

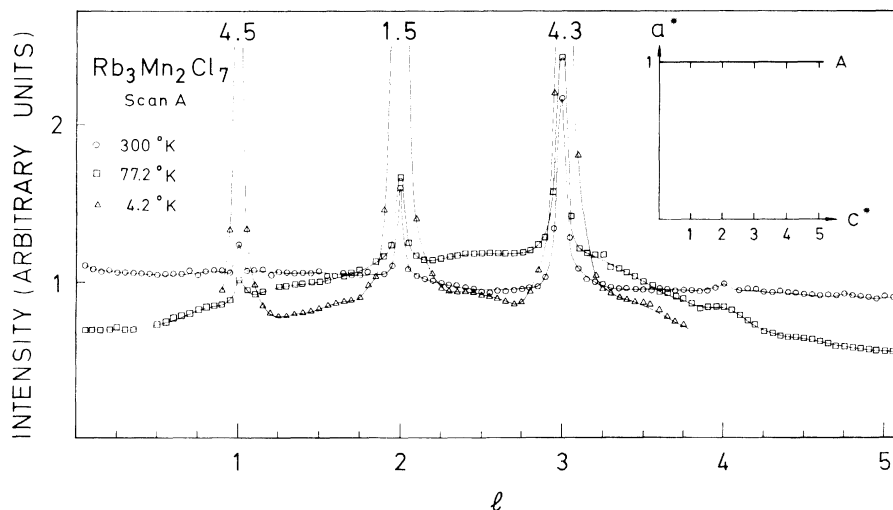


FIG. 6. Scans in reciprocal space along the rod  $(1, 0, l)$ .

by the appearance of rods of coherent intensity in the reciprocal space, perpendicular to the layers.<sup>13</sup> In the  $n=1$  case, the intensity along the rod decays only owing to the form factor but is otherwise constant. In  $\text{Rb}_3\text{Mn}_2\text{Cl}_7$  the constant structure factor (along the rod) will, however, be multiplied by  $\sin \pi l t$  due to intrapair interference of the scattered neutrons, where  $t$  is the interlayer distance (in units of  $c_m$ ) within the pair. In  $\text{Rb}_3\text{Mn}_2\text{Cl}_7$  we have  $t = 1 - 2z(\text{Mn}^{2+}) = 0.202$  (Table III) and the first maxima should appear at  $2l_{\max} = 1$ , namely,  $l_{\max} = 2.48$ . The  $A$  scan (Fig. 6) along the rod  $10l$  with the sample at  $77.2^\circ\text{K}$  ( $T_N + 12.7$ ) is in a complete agreement with this expectation. The peak in the  $B$  scan, across the rod (Fig. 7) is as expected from a rod.

The critical scattering from single layered ( $n=1$ )

structures exists at temperatures as high as  $1.5T_N$  above  $T_N$ .<sup>4</sup> In three-dimensional crystals, on the other hand, critical scattering is expected to exist only close to  $T_N$ . The double layered ( $n=2$ ) structures can be considered as having the properties of two- and three-dimensional crystals. Their critical scattering is therefore expected to extend to somewhat less than  $1.5T_N$  above  $T_N$ . This is seen in Fig. 5 where the critical region does not extend beyond  $1.3T_N$ .

#### ACKNOWLEDGMENTS

A discussion with R. J. Birgeneau concerning the modulation along the "rod intensity" is greatly appreciated. Discussions with R. M. Hornreich are gratefully acknowledged.

<sup>1</sup>A. Tressaud, thesis (University of Bordeaux, 1969) (unpublished).

<sup>2</sup>C. Brisi and M. Lucco Borlera, *J. Inorg. Nucl. Chem.* **27**, 2129 (1965).

<sup>3</sup>J. D. H. Donnay and H. M. Ondik, *Crystal Data Determinative Tables* (U. S. Dept. of Commerce, National Bureau of Standards, Washington, D. C., 1973), Vol. II.

<sup>4</sup>L. H. de Jongh and A. R. Miedema, *Adv. Phys.* **23**, 1 (1974).

<sup>5</sup>E. Gurewitz, A. Epstein, J. Makovsky, and H. Shaked, *Phys. Rev. Lett.* **25**, 1713 (1970).

<sup>6</sup>J. Makovsky, A. Zodkevitz, and Z. H. Kalman, *J. Cryst. Growth* **11**, 99 (1971).

<sup>7</sup>M. Amit, A. Horowitz, and J. Makovsky, *Isr. J. Chem.* **10**, 715 (1972).

<sup>8</sup>The weighted  $R$  factor is given by

$$R = \left[ \sum \left( \frac{I_{\text{obs}} - I_{\text{calc}}}{\sigma} \right)^2 \right]^{1/2} / \left[ \sum \left( \frac{I_{\text{obs}}}{\sigma} \right)^2 \right]^{1/2},$$

where  $I_{\text{obs}}$  and  $I_{\text{calc}}$  are the observed and calculated integrated intensities.  $\sigma$  is the experimental error in  $I_{\text{obs}}$ .

<sup>9</sup>W. Opechowski and R. Guccione, in *Magnetism*, edited by G. T. Rado and H. Suhl (Academic, New York, 1965),

Vol. IIa, p. 105.

<sup>10</sup>V. A. Koptsik, Shubnikov Groups (University of Moscow, Moscow, USSR, 1966) (in Russian).

<sup>11</sup>F. Keffer, *Phys. Rev.* **87**, 608 (1952).

<sup>12</sup>It is easily seen that the dipolar energies for a single set of  $n$  layers are:

$$E_{\parallel} = \frac{\mu^2}{a^3} \sum_{k, h=-\infty}^{+\infty} \frac{(-1)^{h+k+l} (h^2 + k^2 - 2l^2)}{(h^2 + k^2 + l^2)^{5/2}}$$

and

$$E_{\perp} = \frac{\mu^2}{a^3} \sum_{k, h=-\infty}^{+\infty} \frac{(-1)^{h+k+l} [l^2 - \frac{1}{2}(h^2 + k^2)]}{(h^2 + k^2 + l^2)^{5/2}}.$$

$E_{\perp} = -1/2 E_{\parallel}$ , where the summation over  $l$  is carried from  $l=0$  to  $l=n-1$  for ions on the lowest layer of the set; from  $l=-1$  to  $l=n-2$  for ions on the next layer, etc.

<sup>13</sup>R. J. Birgeneau, J. H. Guggenheim, and G. Shirane, *Phys. Rev. Lett.* **22**, 720 (1969).